nature genetics

© 2003 Nature Publishing Group http://www.nature.com/naturegenetics

14-3-3ε is important for neuronal migration by binding to NUDEL: a molecular explanation for Miller–Dieker syndrome

Kazuhito Toyo-oka[1], Aki Shionoya[2], Michael J Gambello[1,5], Carlos Cardoso[3,5], Richard Leventer[3,5], Heather L Ward[3], Ramses Ayala[4], Li-Huei Tsai[4], William Dobyns[3], David Ledbetter[3], Shinji Hirotsune[2] & Anthony Wynshaw-Boris[1]

Heterozygous deletions of 17p13.3 result in the human neuronal migration disorders isolated lissencephaly sequence (ILS) and the more severe Miller–Dieker syndrome (MDS). Mutations in *PAFAH1B1* (the gene encoding LIS1) are responsible for ILS and contribute to MDS, but the genetic causes of the greater severity of MDS are unknown. Here, we show that the gene encoding 14-3-3ε (*YWHAE*), one of a family of ubiquitous phosphoserine/threonine–binding proteins, is always deleted in individuals with MDS. Mice deficient in *Ywhae* have defects in brain development and neuronal migration, similar to defects observed in mice heterozygous with respect to *Pafah1b1*. Mice heterozygous with respect to both genes have more severe migration defects than single heterozygotes. 14-3-3ε binds to CDK5/p35-phosphorylated NUDEL and this binding maintains NUDEL phosphorylation. Similar to LIS1, deficiency of 14-3-3ε results in mislocalization of NUDEL and LIS1, consistent with reduction of cytoplasmic dynein function. These results establish a crucial role for 14-3-3ε in neuronal development by sustaining the effects of CDK5 phosphorylation and provide a molecular explanation for the differences in severity of human neuronal migration defects with 17p13.3 deletions.

Heterozygous deletions in human chromosome 17p13.3 result in two clinically distinct disorders with classical lissencephaly (smooth brain), a severe neuronal migration defect associated with profound mental retardation and epilepsy: ILS and MDS. Children with either of these disorders have agyria and pachygyria that result from disorganization of cortical layering during neuronal migration starting at 9–13 weeks of gestation[1]. The spectrum of lissencephaly varies from complete or nearly complete absence of cerebral convolutions or agyria (grades 1 and 2) to abnormally wide convolutions or pachygyria (grade 4) to normal convolutions separated by shallow sulci beneath which is a variable band of misplaced neurons known as a subcortical band heterotopia (grade 6). Intermediate grades consist of mixed agyria-pachygyria (grade 3) and mixed pachygyria–subcortical band heterotopia (grade 5). ILS consists of variable degrees of severity of lissencephaly with no other associated defects. MDS consists of generally more severe classical lissencephaly as well as craniofacial defects, such as prominent forehead, microcephaly, small jaw, small nose, thin vermilion border of the lip and micrognathia[1–3]. Overlapping heterozygous deletions of 17p13.3 occur in individuals with both ILS and MDS[2–5], suggesting that a gene associated with classical lissencephaly was located in the region of overlapping deletions. *PAFAH1B1* (also called *LIS1*) was identified as a gene consistently deleted in the overlapping region[6], and intragenic deletions and point mutations in individuals with ILS without 17p13.3 deletions confirmed that *PAFAH1B1* is the gene associated with ILS[7].

Additional support for an important role for LIS1 dosage in neuronal migration comes from model organisms. Mice with low doses of *Pafah1b1* had disorganized cortical layers, hippocampus and olfactory bulb owing to defects in cell-autonomous neuronal migration (these mice are a good model for ILS[8,9]), whereas complete loss of LIS1 results in peri-implantation lethality[8,10]. LIS1 is part of a highly conserved evolutionary pathway that regulates cytoplasmic dynein motor function (reviewed in refs. 11,12). This pathway was first outlined in *Aspergillus*, where it participates in nucleokinesis during hyphal stalk formation (reviewed in refs. 11,13), and is functionally conserved in *Drosophila* and mammals. We previously reported that NUDEL, a homolog of NudE from *Aspergillus nidulans*, is a LIS1-binding protein that participates with LIS1 in the regulation of cytoplasmic dynein heavy chain function through phosphorylation by CDK5/p35 (refs. 14,15), a complex known to be essential for neuronal migration (refs. 16,17 and reviewed in ref. 12).

[1]Departments of Pediatrics and Medicine, UCSD Cancer Center, University of California, San Diego School of Medicine, 9500 Gilman Drive, Mailstop 0627, La Jolla, California 92093-0627, USA. [2]Center for Genome Medical Science, Saitama Medical School PRESTO, Japan Science and Technology Corporation, Inariyama 1397-1, Yamane, Hidaka City, Saitama 350-1241, Japan. [3]Department of Human Genetics, The University of Chicago, 924 E. 57th St., Rm. R113, Chicago, Illinois 60637-1470, USA. [4]Department of Pathology, Howard Hughes Medical Institute, Harvard Medical School, 200 Longwood Avenue, Boston, Massachusetts 02115, USA. [5]Present addresses: Department of Pediatrics, Division of Medical Genetics, The University of Texas Health Science Center at Houston Medical School, Houston, Texas 77030, USA (M.J.G.); INSERM U491, Faculte de Medecine La Timone, 27 Bd. Jean Moulin, 13385 Marseille Cedex 05, France (C.C.); Department of Neurology & Murdoch Children's Research Institute, Royal Children's Hospital, Parkville, Victoria 3052, Australia (R.L.). Correspondence should be addressed to A.W.-B. (awynshawboris@ucsd.edu) or S.H. (shinjih@saitama-med.ac.jp).

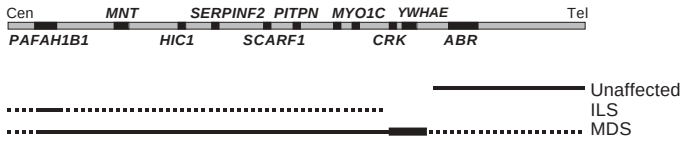

Figure 1 Extent of deletion and brain phenotype of individuals with ILS and MDS. Schematic representation of human 17p13.3 showing the extent of deletion in individuals with MDS or ILS and in unaffected individuals, summarized from ref. 25. The top line shows the relative location of a subset of genes from centromeric to telomeric ends of this region (*PAFAH1B1*, *MNT*, *HIC1*, *SERPINF2*, *SCARF1*, *PITPN*, *MYO1C*, *CRK*, *YWHAE* and *ABR*) in black. At the bottom, the extent of deletions seen in all affected individuals are indicated by solid lines, and the thicker line denotes the size of the region critical for MDS. Dotted lines indicate deletions that can occur in these disorders without added phenotypes beyond deletions in the critical region.

Recent studies have identified a correlation in the pattern of deletions in ILS and MDS. About 40% of individuals with ILS have submicroscopic deletions of 17p13.3 that include *PAFAH1B1*, whereas 25% of individuals with ILS have intragenic mutations of *PAFAH1B1* (refs. 18,19). All individuals with MDS have larger microscopic or submicroscopic deletions of 17p13.3 that include *PAFAH1B1*, and all individuals with deletions extending from *PAFAH1B1* to the 17p telomere had MDS rather than ILS[5]. Thus, although reduction of LIS1 dosage is responsible for the neuronal migration defects in ILS and is probably important for at least some portion of those defects in MDS, recent results suggest that other genes that have not yet been identified are responsible for the more severe lissencephaly and craniofacial defects of MDS. The region is now completely sequenced in human and mouse, and several genes at 17p13.3 have been identified, one of which (*YWHAE*) encodes 14-3-3ε, a member of the 14-3-3 protein family.

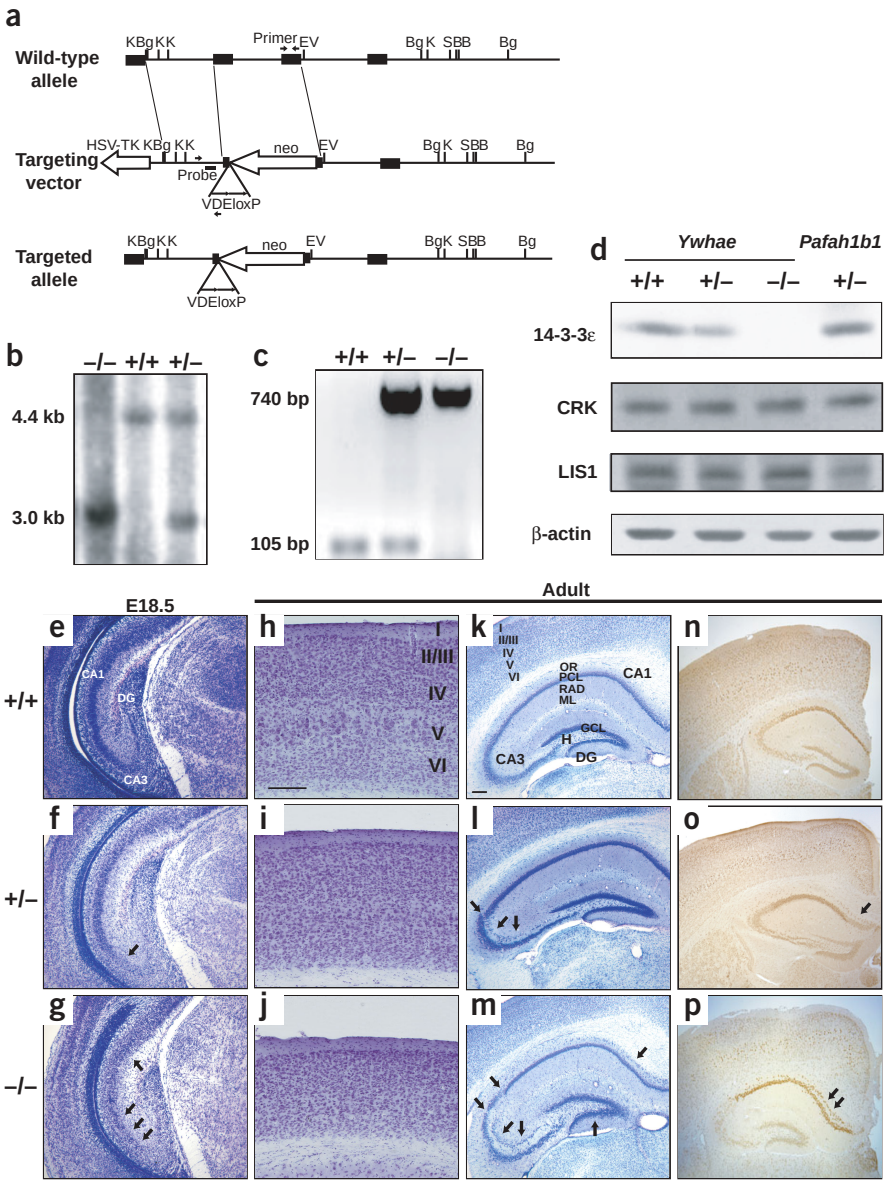

Figure 2 Production and phenotype of 14-3-3ε-mutant mice. (**a**) Summary of targeting strategy for the *Ywhae* locus. Diagrammatic representation of the targeting vector and genomic locus. Exons are represented by black boxes. Arrows indicate primers used for genotyping with PCR, and the probe used for Southern-blot analysis is shown as a bar. K, *Kpn*I; Bg, *Bgl*II; EV, *Eco*RV; S, *Sal*I; B, *Bam*HI; VDE, a 34-bp rare cutting enzyme; *lox*P, site for Cre recombinase; *neo*, neomycin resistance gene; HSV-TK, herpes simplex virus thymidine kinase gene. (**b**) Southern-blot analysis of tail DNA from wild-type ($Ywhae^{+/+}$; +/+), heterozygous mutant ($Ywhae^{+/-}$; +/–) and homozygous mutant ($Ywhae^{-/-}$; –/–) mice. (**c**) PCR genotyping of 14-3-3ε-deficient mice. PCR was done on tail DNA isolated from progeny of heterozygous intercrosses. Product sizes (bp) are indicated. (**d**) Western-blot analysis of adult brain lysates were immunoblotted with antibodies specific for 14-3-3ε, CRK or LIS1, with β-actin used as loading control. (**e–g**) Nissl staining of E18.5 hippocampus shows the disorganization of the pyramidal cell layer in mutant mice (representative of $n = 3$ for each genotype). CA1 and CA3, pyramidal cell regions; DG, dentate gyrus; arrows, disorganization of the pyramidal cell layer. (**h–j**) Nissl staining of adult cortex from wild-type and mutant adults (representative of $n = 2$–3 per genotype). I–VI, cortical layers. (**k–m**) Nissl staining of inbred adult hippocampus of wild-type and mutant mice (representative of $n = 5$ for each genotype). Arrows indicate ectopic cells and splitting in CA3 as observed in $Ywhae^{+/-}$ (**l**) and $Ywhae^{-/-}$ mutants (**m**). I–VI, cortical layers; CA1 and CA3, pyramidal cell regions; DG, dentate gyrus; GCL, granule cell layer; H, hilus; ML, molecular layer; OR, stratum oriens; PCL, pyramidal cell layer; RAD, stratum radiatum. Scale bar, 75 μm (**h**,**k**). (**n–p**) Immunostaining with antibody to Tst-1 showed a second layer of pyramidal cells in CA1 (arrows in **o**,**p**) in both $Ywhae^{+/-}$ and $Ywhae^{-/-}$ mutants (representative of $n = 5$–6 for each genotype). All sections in this figure came from embryos and adults of mixed background.

© 2003 Nature Publishing Group http://www.nature.com/naturegenetics

14-3-3s are ubiquitous proteins that are highly conserved from bacteria to humans and plants and have several molecular and cellular functions (reviewed in refs. 20–22). Most notably, 14-3-3 proteins bind to phosphoserine/phosphothreonine motifs in a sequence-specific manner (RSxpS/TxP or R′pS/TxP; refs. 23,24). More than 100 14-3-3 binding partners involved in signal transduction, cell cycle regulation, apoptosis, stress responses and malignant transformation have been identified. There are at least seven distinct genetic loci (sometimes referred to as isoforms) in mammals, ten in plants and two each in yeast, *Drosophila melanogaster* and *Caenorhabditis elegans*. The 14-3-3 proteins form homo- and heterodimers, and there is redundancy of the binding specificity and function of different 14-3-3 proteins due to their highly similar amino acid sequence and tertiary structure (reviewed in refs. 20,22). 14-3-3 proteins can regulate target protein function by several mechanisms, including alteration of target protein binding to other partners, regulation of subcellular localization, alteration of catalytic activity, protection from proteolysis or dephosphorylation and bridging of two targets as an adapter or scaffold[22]. Although the molecular and cellular functions of 14-3-3 proteins have been well studied, there have been fewer studies addressing the *in vivo* role of 14-3-3s.

Here, we show that *YWHAE* encoding 14-3-3ε is deleted in all individuals with MDS. Moreover, we show that 14-3-3ε is essential for normal brain development and neuronal migration in the mouse. This function of 14-3-3ε seems to be accomplished at least in part by binding to CDK5/p35 phosphorylated NUDEL to maintain NUDEL phosphorylation. These data suggest that 14-3-3ε has an important role in mammalian neuronal migration and provide an explanation for the severity of defects in neuronal migration in MDS.

RESULTS

Haploinsufficiency of *YWHAE* and severe human lissencephaly

We recently published a complete study of these findings in individuals with ILS and MDS[25], and we will briefly summarize some of the salient points here. To determine the genes deleted consistently in MDS, we first determined the extent of heterozygous deletion by fluorescence *in situ* hybridization analysis in cells from individuals with ILS and MDS compared with the severity of the clinical lissencephaly phenotype. We made somatic cell hybrids that contained the deleted chromosome from individuals with ILS and MDS without complete 17p terminal deletions, and we used PCR assays to assess the presence or deletion of eight genes on 17p. The genes *PAFAH1B1*, *SCARF1*, *PITPN*, *MYO1C*, *CRK*, *YWHAE* and *ABR* span over 1 Mb from the centromeric to telomeric ends of the MDS region[25]. We compared the extent of deletions in these individuals and in unaffected individuals with 17p telomeric deletions and normal phenotype (**Fig. 1**). Individuals with grade 2–3 lissencephaly (ILS) had large submicroscopic deletions affecting *PAFAH1B1* and a variable number of genes telomeric to *PAFAH1B1* but never including *CRK* and *YWHAE*. By comparison, individuals with MDS with grade 1 lissencephaly (and characteristic facial features of MDS) had visible or large submicroscopic deletions affecting *PAFAH1B1* and many telomeric genes, including *YWHAE*. Two of these individuals had a deletion that

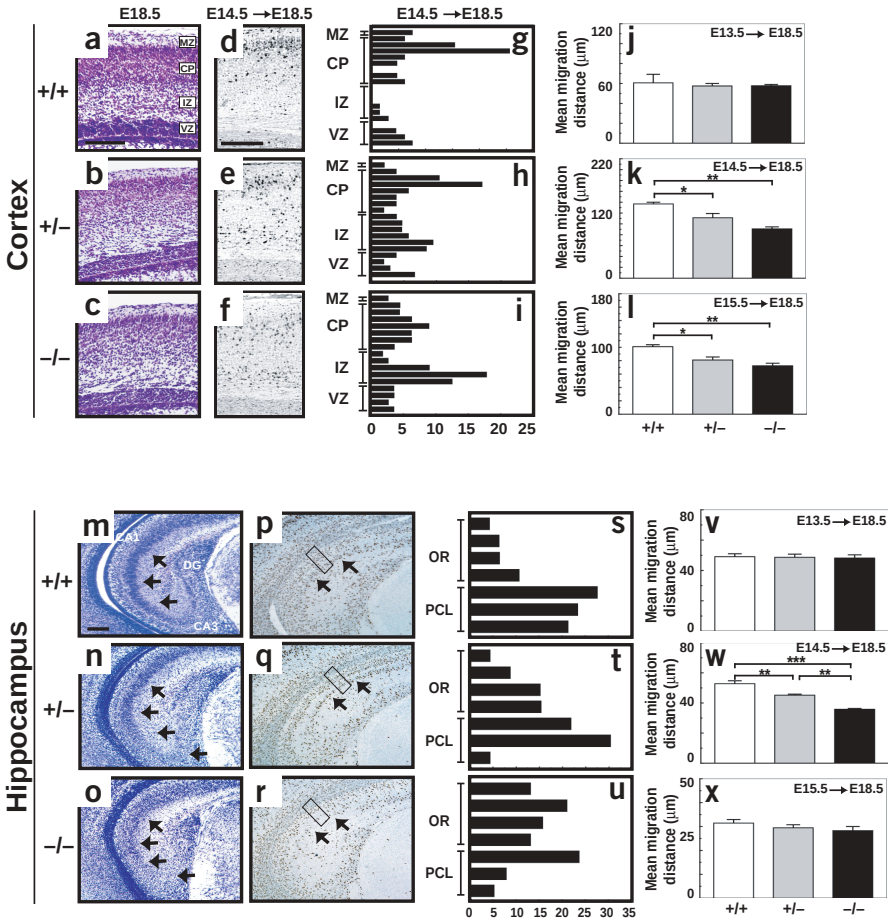

Figure 3 BrdU birthdating analysis identifies neuronal migration defects in 14-3-3ε-deficient mice. Nissl staining of cortex (**a–c**) and hippocampus (**m–o**) from wild-type (*Ywhae*$^{+/+}$; +/+), heterozygous (*Ywhae*$^{+/-}$; +/–) and homozygous mutant (*Ywhae*$^{-/-}$; –/–) embryos at E18.5 from pregnant dams of mixed background injected with BrdU at E14.5. CA1 and CA3, pyramidal cell regions; CP, cortical plate; DG, dentate gyrus; IZ, intermediate zone; MZ, marginal zone; VZ, ventricular zone; arrows, pyramidal cell layer. Scale bars: 75 μm (**a**,**d**); 50 μm (**m**). Adjacent sections are shown of BrdU-labeled cells in cortex (**d–f**) and hippocampus (**p–r**). (**g–i**) Quantitative analysis of the percentage of BrdU labeled cells (*x* axis) in 10-μm bins precisely adjacent to the cortical sections and grouped by region (MZ, CP, IP and VZ; along the *y* axis). The number of bins in *Ywhae*$^{+/+}$, *Ywhae*$^{+/-}$ and *Ywhae*$^{-/-}$ mice was 19, 18 and 17 bins, respectively. Note the shift downward toward the ventricular zone as 14-3-3ε dosage was reduced. (**s–u**) Quantitative analysis of the percentage of BrdU-labeled cells (*x* axis) in 10-μm bins of the boxed areas from **p–r** from stratum oriens (OR) through the pyramidal cell layer (PCL), as indicated along the *y* axis. Note the shift upward toward to ventricular zone at the top of stratum oriens as 14-3-3ε dosage was reduced. Mean migration distance was determined for all BrdU-labeled cells in ten sections each of the cortex (**j–l**) and stratum oriens and pyramidal cell layer of hippocampus (**v–x**) of four E18.5 embryos for each genotype and each day of BrdU injection at E13.5 (**j**,**v**), E14.5 (**k**,**w**) and E15.5 (**l**,**x**). Error bars indicate s.e.m. and significance is indicated by asterisks (*$P < 0.05$, **$P < 0.01$, ***$P < 0.001$).

© 2003 Nature Publishing Group http://www.nature.com/naturegenetics

included *YWHAE* but not *ABR*, the next more telomeric gene in this region (**Fig. 1**). Individuals with further telomeric deletions had no greater severity of the MDS phenotype. These findings suggest that deletions resulting in haploinsufficiency of *PAFAH1B1* through *YWHAE* on 17p13.3 are sufficient for the severe brain and craniofacial phenotypes of individuals with MDS and that *CRK* and *YWHAE* may be important in neuronal migration.

Targeted disruption of *Ywhae*

To determine if loss of function of *Ywhae in vivo* results in developmental defects in the brain, we generated mice lacking a functional gene (**Fig. 2a**). We identified a targeted embryonic stem cell (ES) clone in which exons 2 and 3 of *Ywhae* were partially replaced by *neo*, injected it into C57BL/6J blastocysts and introduced the mutation into the germ line as mixed (129/S6 and NIH Black Swiss) and inbred (129/S6) lines. Mice heterozygous with respect to *Ywhae* (*Ywhae*$^{+/-}$) were outwardly normal and fertile, and we bred them together to produce homozygous null mice (*Ywhae*$^{-/-}$). We genotyped mice by Southern-blot analysis (**Fig. 2b**) and PCR (**Fig. 2c**). Virtually all *Ywhae*$^{-/-}$ mice died at birth with slightly lower weight than wild-type mice (data not shown). Only about 2.5% of *Ywhae*$^{-/-}$ mice in the mixed background and less than 1% of inbred mice survived to adulthood and looked small but were otherwise outwardly normal (data not shown). There was no expression of endogenous 14-3-3ε in brain lysates from *Ywhae*$^{-/-}$ mice by immunoblot analysis, whereas lysates from *Ywhae*$^{+/-}$ mice had about half the levels of 14-3-3ε protein measured in wild-type mice (**Fig. 2d**). In addition, loss of 14-3-3ε had no effect on CRK or LIS1 protein levels, and there was no reduction of 14-3-3ε protein levels in brain lysates from *Pafah1b1* heterozygotes (**Fig. 2d**).

14-3-3ε-deficient mice have hippocampal and cortical defects

Because nearly all 14-3-3ε-deficient mice died at birth, we examined tissues from embryonic day (E) 18.5 *Ywhae*$^{+/+}$, *Ywhae*$^{+/-}$ and *Ywhae*$^{-/-}$ mixed background mice; we observed similar results in inbred mice (data not shown). Except for the brain, all other tissues were similar in mutants and wild-type mice. Compared to *Ywhae*$^{+/+}$ mice, all *Ywhae*$^{+/-}$ and *Ywhae*$^{-/-}$ mice had hippocampal defects (**Fig. 2e–g**) and thinning of the cortex (data not shown). The pyramidal cell layer of the hippocampus of *Ywhae*$^{+/-}$ mice was mildly disorganized and less cellular. These phenotypes were more severe in brains from *Ywhae*$^{-/-}$ mutants.

We also observed dose-dependent cortical thinning in brains of adult *Ywhae*$^{+/-}$ and surviving *Ywhae*$^{-/-}$ mutant mice in a mixed background (**Fig. 2h–j**). Cortical thickness was significantly less in brains from adult *Ywhae*$^{+/-}$ mice (340.4 ± 3.91 μm) compared with *Ywhae*$^{+/+}$ mice (382.7 ± 3.91 μm) and even less in brains from surviving *Ywhae*$^{-/-}$adults (276.6 ± 5.51 μm). We detected no differences in proliferation in the ventricular zone of brains from wild-type and mutant mice between E12.5 and E15.5 by measuring uptake of 5-bromo-2-deoxyuridine

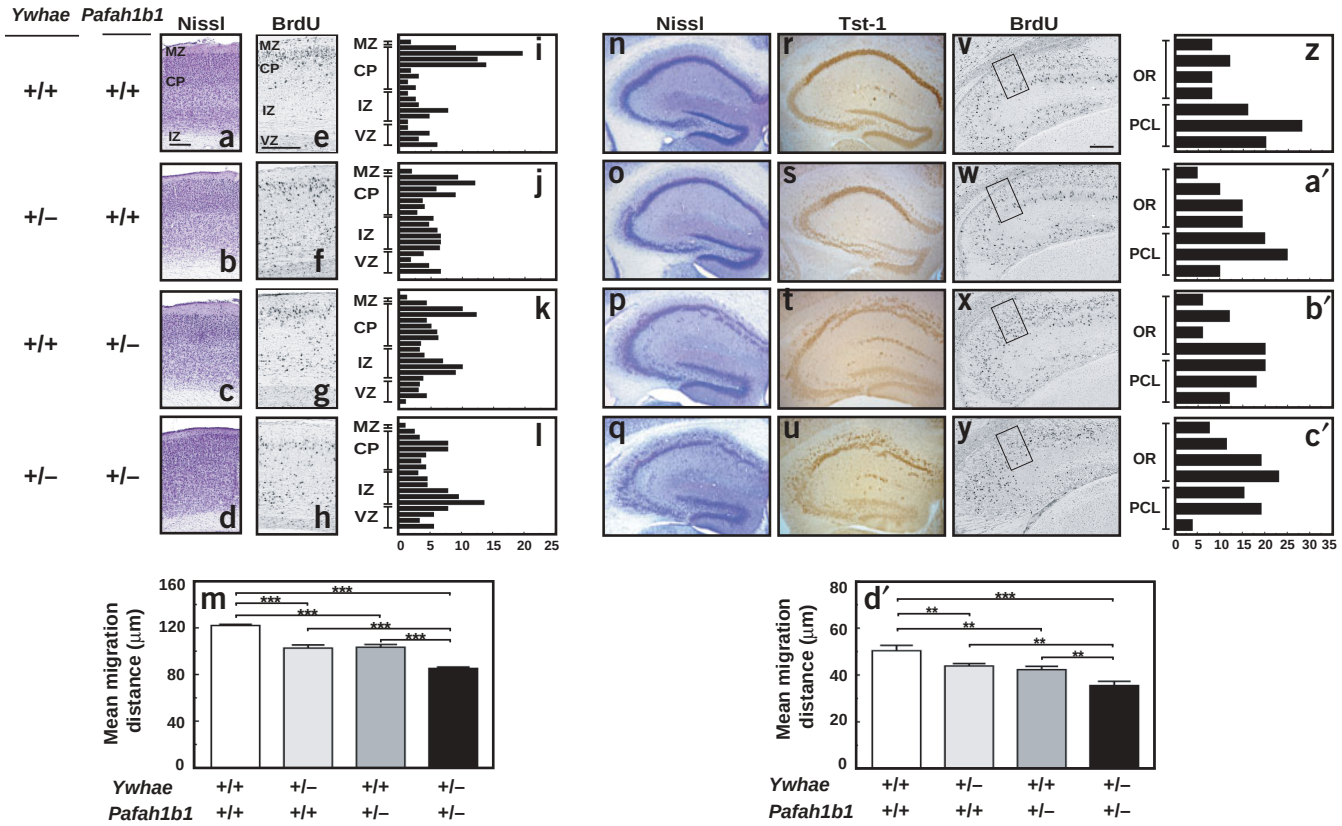

Figure 4 Genetic link between *Ywhae* and *Pafah1b1* during cortical and hippocampal migration. Nissl staining (**a–d**, **n–q**), BrdU birthdating (**e–h**, **v–y**) with bin analysis as in **Figure 3** (**i–l**, **z–c′**) and Tst-1 marker analysis (**r–u**) of cortex (**a–l**) and hippocampus (**n–c′**) from wild-type (**a**,**e**,**i**,**n**,**r**,**v**,**z**), *Ywhae*$^{+/-}$ *Pafah1b1*$^{+/+}$ (**b**,**f**,**j**,**o**,**s**,**w**,**a′**), *Ywhae*$^{+/+}$ *Pafah1b1*$^{+/-}$ (**c**,**g**,**k**,**p**,**t**,**x**,**b′**) and *Ywhae*$^{+/-}$ *Pafah1b1*$^{+/-}$ (**d**,**h**,**l**,**q**,**u**,**y**,**c′**) mice in an inbred 129/SvEv background. Mice were injected with BrdU at E14.5 and killed at E18.5. Scale bars, 37.5 μm (**a**), 75 μm (**e**), 50 μm (**v**). The boxes in **v–y** denote the regions where 10-μm bins were quantified in stratum oriens (OR) and the pyramidal cell layer (PCL). Mean migration distance was determined for all BrdU-labeled cells in ten sections each of the cortex (**m**) and stratum oriens and pyramidal cell layer of hippocampus (**d′**) of four E18.5 embryos for each genotype and after BrdU injection at E14.5. Error bars indicate s.e.m. and significance is indicated by asterisks (**$P < 0.01$, ***$P < 0.001$).

© 2003 Nature Publishing Group http://www.nature.com/naturegenetics

(BrdU) for S phase and staining for mitotic cells positive for phosphorylated histone H3 (data not shown). We observed a small but significant three-fold increase in the number of TUNEL-positive cells in brains from *Ywhae*$^{-/-}$ versus *Ywhae*$^{+/+}$ littermates at E12.5 (data not shown), suggesting that the thinned cortex of mutant mice may be due to more cell death rather than less proliferation of neuronal precursors.

We also observed hippocampal defects in brains of adult *Ywhae*$^{+/-}$ and surviving *Ywhae*$^{-/-}$ mutant mice of mixed background (**Fig. 2k–m**). In the CA1 region of the hippocampus of *Ywhae*$^{-/-}$ mutants, the stratum pyramidale had a two-layered appearance with ectopic cells present in stratum oriens, whereas in the CA3 region, this layer was diffusely packed and split with heterotopic pyramidal cells located throughout the entire hippocampal subfield, including stratum oriens and stratum radiatum. Granule cells were loosely packed in the dentate gyrus. We used Tst-1, a neuronal marker expressed in the pyramidal cells of the CA1 region in hippocampus and in layers II,III and V of the cortex[26], to examine cortical layering. The CA1 pyramidal cells of mutant mice were clearly defective, but the large pyramidal cells in layer V were correctly positioned in mice of both genotypes, indicating no cortical layer inversion (**Fig. 2n–p**).

Neuronal migration defects in mice with mutations in *Ywhae*

Similar dose-dependent brain defects have been observed in mice with mutations in *Pafah1b1* due to abnormal neuronal migration[8,9,27]. To determine whether mice with mutations in *Ywhae* had neuronal migration defects, we carried out BrdU birthdating analysis. We injected pregnant dams from heterozygous mixed background crosses with BrdU on E13.5, E14.5 and E15.5 and detected BrdU-positive cells in coronal sections of brains from mice of all three genotypes on E18.5 (because *Ywhae*$^{-/-}$ mice die at birth). A single example of BrdU injection at E14.5 is presented for each genotype. Sections from cortex (**Fig. 3a–c**) and hippocampus (**Fig. 3m–o**) stained with cresyl violet showed morphology, and adjacent sections showed BrdU-labeled cells (**Fig. 3d–f,p–r**). To quantify migration, we divided the brain regions into 10-μm bins and determined the percentage of labeled cells located in each bin in the cortex (**Fig. 3g–i**) and hippocampus (**Fig. 3s–u**) as indicated for each genotype. The cortex and hippocampus were formed in an inside-out fashion, but as the dose of 14-3-3ε was reduced, the distribution of labeled cells was shifted downward toward the ventricular zone in the cortex (**Fig. 3g–i**), whereas BrdU labeling was more diffusely localized in the hippocampus (**Fig. 3s–u**).

We calculated average mean neuronal migration distances for labeled cortical cells as well as cells in stratum oriens and the pyramidal cell layer in ten sections from four brains per genotype at each day of BrdU injection. We found similar mean migration distances of BrdU-labeled cortical cells in mice of all three genotypes injected at E13.5 (**Fig. 3j**), but migration distances were significantly shorter in a dose-dependent fashion in brains from *Ywhae*$^{+/-}$ and *Ywhae*$^{-/-}$ mice labeled at E14.5 and E15.5 than in wild-type brains (**Fig. 3k,l**). Likewise, we observed similar mean migration distances in the hippocampus at E13.5 (**Fig. 3v**) and E15.5 (**Fig. 3x**) in mice of all three genotypes, but these distances were significantly shorter in a dose-dependent fashion in brains from *Ywhae*$^{+/-}$ and *Ywhae*$^{-/-}$ mice labeled at E14.5 than in wild-type brains (**Fig. 3w**). Thus, mice deficient for 14-3-3ε have slower neuronal

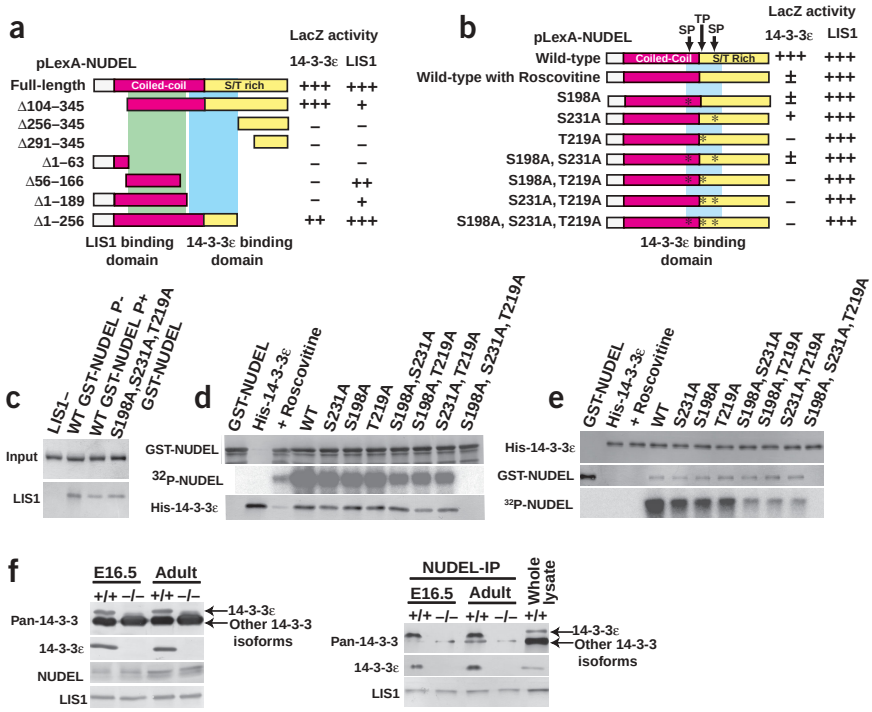

Figure 5 Interaction of 14-3-3ε with NUDEL. (**a**) Determination of the interaction domain of 14-3-3ε with NUDEL in the Ser/Thr region (blue in **a** and **b**) compared with the interaction domain of LIS1 with NUDEL in the coiled-coil region (green). Regions of NUDEL used for the fusion protein are indicated on the left. LacZ activity of each combination was scored in a semi-quantitative fashion (right). (**b**) Effect of the Pho85/CDK5 inhibitor roscovitine or point mutations of CDK5 phosphorylation sites in NUDEL for yeast two-hybrid binding to 14-3-3ε or LIS1. Point mutations introduced are indicated on the left. LacZ activity of each combination was scored in a semi-quantitative fashion (right). (**c**) *In vitro* interaction assays using recombinant proteins for LIS1 with GST-tagged NUDEL, P-NUDEL (phosphorylated by CDK5/p35 in the presence of [γ-^{32}P]-ATP) and the triple mutant (S198A, T219A, S231A) NUDEL, measured by pull-down with glutathione-sepharose beads. (**d**,**e**) Effects of mutations introduced to CDK5 phosphorylation sites were analyzed by *in vitro* interaction assays using recombinant proteins. Wild-type (WT) and mutant NUDEL (as GST fusions) were phosphorylated by recombinant CDK5/p35 in the presence of [γ-^{32}P]-ATP and incubated with His-tagged 14-3-3ε. Proteins were pulled down by glutathione-sepharose beads (**d**) or Ni beads (**e**). Adsorbates were analyzed by immunoblotting with antibody to GST (GST-NUDEL), antibody to His (His-14-3-3ε) and autoradiography (^{32}P-NUDEL). Above the panels, GST-NUDEL and His-14-3-3ε lanes refer to interaction controls using only these proteins, and +Roscovitine indicates that NUDEL phosphorylation by CDK5/p35 was inhibited in the presence of roscovitine. The introduced mutations are indicated above the lanes. (**f**) Left, Western-blot analysis of lysates from E16.5 and adult brains using a pan-14-3-3 antibody, a 14-3-3ε-specific antibody and NUDEL and LIS1 antibodies. 14-3-3ε is larger than other 14-3-3 isoforms. Right, co-immunoprecipitation of 14-3-3ε, other 14-3-3 isoforms and LIS1 by NUDEL from E16.5 and adult brains lysates using an antibody to NUDEL.

© 2003 Nature Publishing Group http://www.nature.com/naturegenetics

migration without cortical layer inversion. These defects were similar to those found in mice with mutations in *Pafah1b1* and show that 14-3-3ε is required for normal migration of hippocampal and cortical neurons.

Ywhae and *Pafah1b1* genetically interact in the brain

Because mice with mutations in *Pafah1b1* and *Ywhae* both have dose-dependent defects in brain development and migration, we determined whether there were genetic interactions between these genes. Inbred mice heterozygous with respect to either *Pafah1b1* or *Ywhae* were mated to decrease any potential variability due to mixed backgrounds. We examined the cortical and hippocampal migration phenotypes of mice of all four resulting genotypes by BrdU birthdating analysis with injection at E14.5 and analysis at E18.5, as described above. We observed slowing of cortical migration (indicated by a downward shift in distribution of labeled cells) in mice heterozygous with respect to either *Ywhae* (**Fig. 4b**,**f**,**j**) or *Pafah1b1* (**Fig. 4c**,**g**,**k**) compared with wild-type mice (**Fig. 4a**,**e**,**i**). Migration was even slower in double heterozygotes (**Fig. 4d**,**h**,**l**). In the hippocampus of wild-type mice, there was a distinct packed layer of pyramidal cells (**Fig. 4n**,**r**). We observed a mild defect in the CA3 region of *Ywhae* heterozygous mice, with heterotopic pyramidal cells and splitting of the stratum pyramidale (**Fig. 4o**,**s**). As previously described[8,27], pyramidal cell layering in *Pafah1b1* heterozygous mice was especially disorganized in the CA1 region, though the CA3 region was also involved (**Fig. 4p**,**t**). In double heterozygous mice, we observed more severe abnormalities of pyramidal cell packing throughout all hippocampal subfields (**Fig. 4q**,**u**). BrdU birthdating (**Fig. 4v–y**) and quantitative bin analysis (**Fig. 4z–c′**) confirmed this order of severity of migration in the hippocampus among these genotypes. We calculated mean migration distances as above and found that there was a significant slowing of migration in the cortex (**Fig. 4m**) and hippocampus (**Fig. 4d′**) of double heterozygotes compared with single heterozygotes and wild-type mice. Taken together, these data suggest that *Ywhae* genetically interacts with *Pafah1b1* during brain development and neuronal migration.

14-3-3ε directly binds NUDEL

The similarity in phenotype in mice with mutations in *Ywhae* and *Pafah1b1* and the genetic interaction between *Ywhae* and *Pafah1b1* suggested that the proteins they encode, 14-3-3ε and LIS1, respectively, are in the same pathway. Yeast two-hybrid screening carried out to further define proteins important for NUDEL function provided evidence for this notion. Full-length mouse NUDEL was used as bait to screen 11×10^6 independent transformants from a mouse fetal brain library. Sixty-seven colonies contained LIS1, providing a positive control for the screen. Notably, 156 other clones encoded five 14-3-3 family members (14-3-3ε, 14-3-3τ, 14-3-3ζ, 14-3-3γ and 14-3-3α/β), with the greatest number of colonies represented by 14-3-3ε (87 of 156; 56%).

To determine the region of NUDEL that binds to 14-3-3ε, we carried out directed yeast two-hybrid interaction assays using several truncated NUDEL expression constructs (**Fig. 5a**). LIS1 binds to the coiled-coil region of NUDEL (amino acids 56–166), whereas a different region of NUDEL (amino acids 189–256) was required for binding of 14-3-3ε. Three specific phosphorylation sites (Ser198, Thr219 and Ser231) and two weak phosphorylation sites (Ser242 and Thr245) for

© 2003 Nature Publishing Group http://www.nature.com/naturegenetics

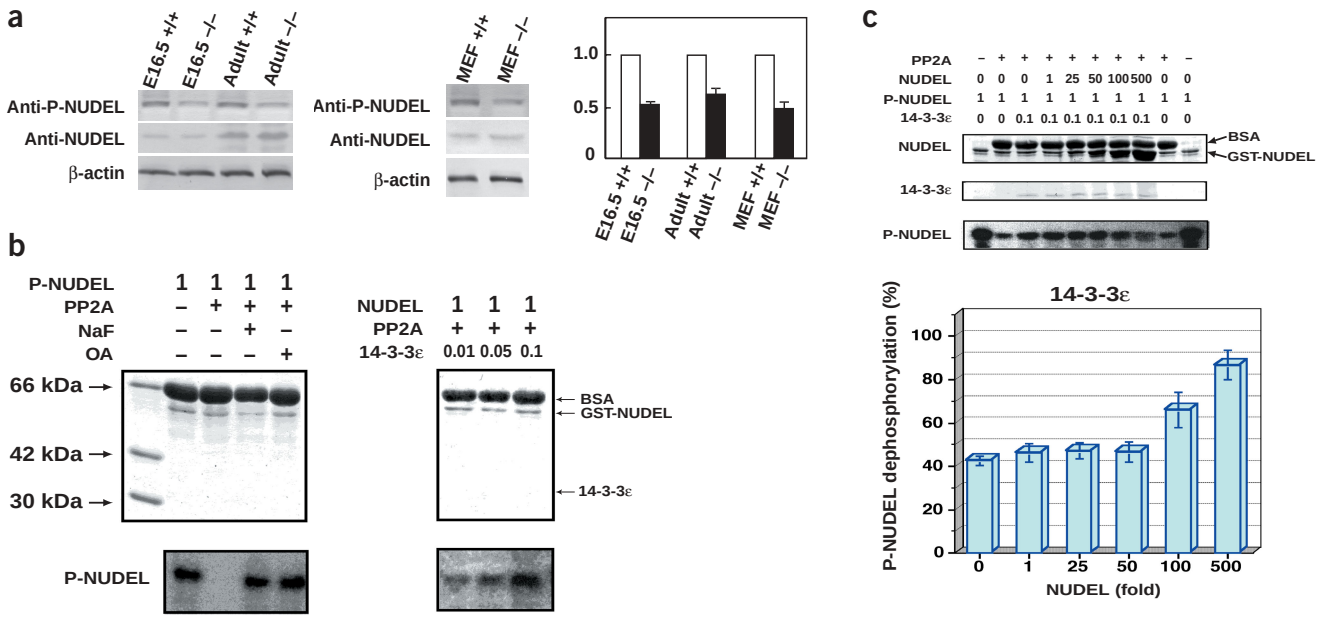

Figure 6 14-3-3ε sustains NUDEL phosphorylation and protects it from phosphatase. (**a**) Representative western-blot analysis of lysates from E16.5 brains, adult brains and MEFs from wild-type (*Ywhae*$^{+/+}$; +/+) and 14-3-3ε-deficient (*Ywhae*$^{-/-}$; –/–) mice, using antibody against P-NUDEL, against NUDEL or against β-actin as loading control. Densitometry analysis of western-blot data for these ages and genotypes, expressed relative to wild-type protein levels ($n = 5$ for E16.5, $n = 3$ for adult brains). (**b**) Inhibition of dephosphorylation of NUDEL by 14-3-3ε. NUDEL phosphorylated by CDK5 in presence of [γ-^{32}P] ATP was incubated with PP2A in the presence of various concentrations of 14-3-3ε (in μg) as indicated above the panels. Reaction mixtures were subjected to SDS–PAGE and then Coomassie staining (top panel). The same filter was subjected to autoradiography (bottom panel). The left panel shows dephosphorylation of P-NUDEL by PP2A and its inhibition by phosphatase inhibitors. The right panel indicates inhibition of PP2A dephosphorylation by 14-3-3ε. BSA, bovine serum albumin; OA, okadaic acid. (**c**) Suppression of the inhibitory effect of dephosphorylation by non-phosphorylated NUDEL. NUDEL phosphorylated by CDK5 in the presence of [γ-^{32}P] ATP was incubated with PP2A in the presence of various concentrations (in μg) of unphosphorylated NUDEL, as indicated above. The proportion of each molecule is described above. After incubation, each reaction mixture was subjected to SDS–PAGE and then Coomassie staining (top panel), immunoblotting by antibody to 14-3-3ε (middle panel) and autoradiography (bottom panel). Radiation activity was measured and quantified as percentage of P-NUDEL dephosphorylation at various ratios of NUDEL/P-NUDEL (bottom graph). BSA, bovine serum albumin.

CDK5/p35 are located in this region of NUDEL[14,15]. This suggests that CDK5/p35 phosphorylation may be crucial for the interaction between NUDEL and 14-3-3ε. Because yeast contains a highly conserved and functional CDK5 homolog, Pho85 (ref. 28), and because NUDEL was phosphorylated in yeast (data not shown), it was possible to examine this hypothesis in yeast. The CDK5 inhibitor roscovitine nearly eliminated the interaction of NUDEL with 14-3-3ε without affecting its interaction with LIS1 (**Fig. 5b**). We produced substitution mutants for each of the CDK5 sites of NUDEL: S198A, T219A and S231A (**Fig. 5b**). Each single or double mutant compromised, and the triple mutant completely eliminated, interaction with 14-3-3ε. These Ser/Thr mutants had no effect on the interaction of LIS1 and NUDEL in yeast (**Fig. 5b**) or as recombinant proteins (**Fig. 5c**). Mutation of two other phosphorylation sites (Ser242, Thr245) located outside of the binding region had only mild effects on interaction (data not shown).

© 2003 Nature Publishing Group http://www.nature.com/naturegenetics

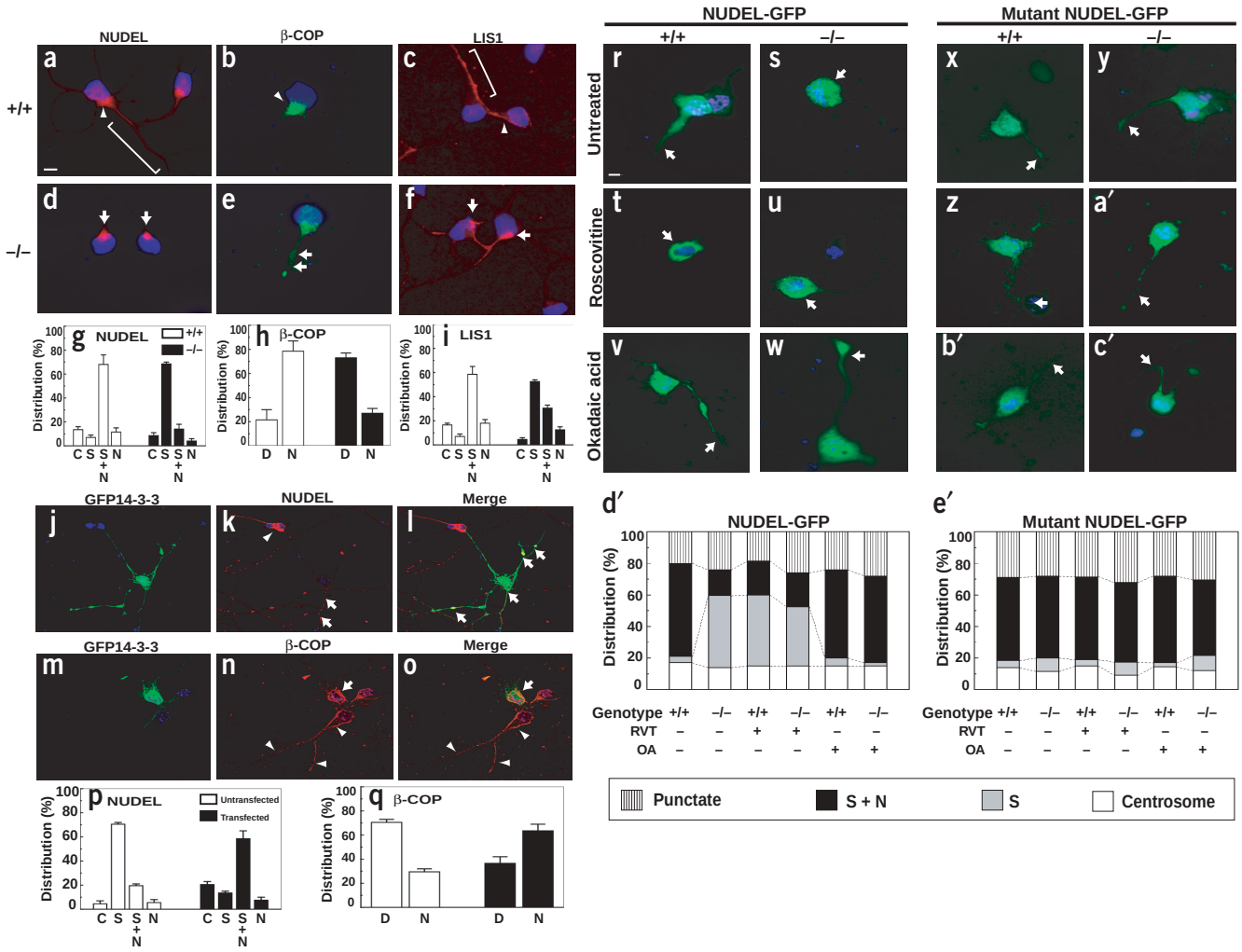

Figure 7 14-3-3ε is important for normal localization of NUDEL, LIS1 and β-COP. (**a–f**) Loss of 14-3-3ε influences distribution of NUDEL (**a**,**d**), β-COP (**b**,**e**) and LIS1 (**c**,**f**) in primary cortical neurons. NUDEL and LIS1 localization (arrowheads and bracket in **a** and **c**) was detected in the soma and neurites (brackets) in wild-type (*Ywhae*$^{+/+}$; +/+) neurons. In 14-3-3ε-deficient (*Ywhae*$^{-/-}$; –/–) neuronal cells, NUDEL and LIS1 were localized in the soma (arrows in **d**,**f**). β-COP was localized throughout the neuron in *Ywhae*$^{-/-}$ cells (**e**, arrows) in contrast to the tight perinuclear localization in wild-type neurons (**b**, arrowhead). Scale bar in **a**, 5 μm. (**g–i**) Quantification of distribution patterns of NUDEL (**g**), β-COP (**h**) and LIS1 (**i**) in cortical neurons each from *Ywhae*$^{+/+}$ and *Ywhae*$^{-/-}$ mice after 2 d in culture. For NUDEL and LIS1 patterns: C, predominantly centrosomal localization; S, soma localization only; S+N, both soma and neurite localization; N, neurite localization only. For β-COP patterns: D, diffuse distribution; N, perinuclear. One hundred cells each of 2–3 mice per genotype were counted. (**j–o**) Transfection of GFP-tagged 14-3-3ε rescued the mislocalization of NUDEL (**j–l**) and β-COP (**m–o**) in primary cortical neurons from *Ywhae*$^{-/-}$ mutants. GFP-14-3-3ε was localized in the soma and neurites (**j**,**m**). NUDEL was diffusely localized in soma and neurites of transfected neurons (**k**, arrows) in contrast to untransfected neurons (**k**, arrowhead). Merged images show colocalization of 14-3-3ε and NUDEL around the nucleus and neurites (**l**, arrows). Similarly, β-COP was tightly localized around the soma in transfected neurons (**n**,**o**, arrow) in contrast to untransfected neurons (**n**,**o**, arrowhead). (**p**,**q**) Bar graphs display the percentage of cells with different distribution patterns of NUDEL (**p**) and β-COP (**q**) in untransfected or GFP-14-3-3ε transfected *Ywhae*$^{-/-}$ mutant neurons. One hundred transfected and untransfected cells were examined. Error bars indicate s.e.m. (**r–c′**) Cortical neuronal cells were transfected with NUDEL-GFP (**r–w**) or triple mutant NUDEL-GFP (**x–c′**) and were untreated (**r**,**s**,**x**,**y**) or treated for 2 d with 1 μM roscovitine (**t**,**u**,**z**,**a′**) or 10 nM okadaic acid (**v**,**w**,**b′**,**c′**). The percentage distribution of localization of NUDEL-GFP (**d′**) and mutant NUDEL-GFP (**e′**) in the two genotypes and with each treatment are shown. One hundred transfected cells of preparations from each of 2–3 mice per treatment were examined. Scale bar in **r**, 5 μm. RVT, roscovitine; OA, okadaic acid.

© 2003 Nature Publishing Group http://www.nature.com/naturegenetics

The yeast two-hybrid data were generally consistent with *in vitro* interaction assays with recombinant glutathione S-transferase (GST)–NUDEL and histidine (His)–14-3-3ε fusion proteins, using glutathione-sepharose beads to pull down GST-NUDEL (**Fig. 5d**) or Ni beads to pull down His-14-3-3ε (**Fig. 5e**). Wild-type NUDEL was phosphorylated *in vitro* by CDK5/p35. Phosphorylated NUDEL (P-NUDEL) interacted strongly with 14-3-3ε. Both phosphorylation and subsequent binding were inhibited by the CDK5 inhibitor roscovitine. Introduction of single, double and triple mutations proportionally reduced the extent of NUDEL phosphorylation by CDK5/p35 and NUDEL/14-3-3ε interaction. Both NUDEL phosphorylation and NUDEL/14-3-3ε interaction were completely abrogated in the triple mutant (S198A, T219A, S231A), suggesting that these three sites are the primary targets of CDK5 phosphorylation and interaction with 14-3-3ε.

We analyzed by western blotting endogenous proteins in E16.5 and adult brain lysates from wild-type (*Ywhae*$^{+/+}$) and 14-3-3ε-deficient (*Ywhae*$^{-/-}$) mice using antibodies that recognize all 14-3-3 isoforms (pan-14-3-3), 14-3-3ε only, LIS1 and NUDEL. 14-3-3ε is slightly higher in molecular weight than the other 14-3-3 isoforms and can be distinguished from the other isoforms with the pan-14-3-3 antibody. 14-3-3ε was present only in brains from *Ywhae*$^{+/+}$ mice, but appreciable amounts of other 14-3-3 isoforms were present in embryonic and adult brain of either genotype (**Fig. 5f**). The amount of NUDEL was greater in the adult than in the embryo, whereas LIS1 was present in equal amounts in brains from E16.5 and adult mice. There was no effect of genotype on amounts of NUDEL or LIS1 at either age. To determine whether 14-3-3ε and NUDEL interact *in vivo*, and whether there was preferential binding of NUDEL to 14-3-3ε compared with other 14-3-3 isoforms, we carried out co-immunoprecipitation with antibody to NUDEL on native proteins followed by western-blot analysis. In brains from *Ywhae*$^{+/+}$ mice, 14-3-3ε was the predominant isoform pulled down with NUDEL (**Fig. 5f**), whereas no 14-3-3ε was detected in immunoprecipitates from *Ywhae*$^{-/-}$ mutant mice. No apparent binding differences to other 14-3-3 isoforms or to LIS1 were detected between *Ywhae*$^{+/+}$ and *Ywhae*$^{-/-}$ mutants. Thus, 14-3-3ε preferentially binds to NUDEL *in vivo*.

14-3-3ε maintains phosphorylation of NUDEL

14-3-3 proteins can have many effects on phosphoproteins, including protection from dephosphorylation[22]. Consistent with such an effect, there were detectable differences in the levels of P-NUDEL in brain and MEF lysates of different genotypes, measured by western-blot analysis with an antibody to P-NUDEL (**Fig. 6a**). There were small amounts of NUDEL protein in brains from *Ywhae*$^{+/+}$ E16.5 embryos, which increased in the adult. Notably, the levels of P-NUDEL were lower in brains from E16.5 or adult *Ywhae*$^{-/-}$ mice, as well as in *Ywhae*$^{-/-}$ MEF lysates. Although MEFs do not contain active CDK5, they do contain CDC2 kinase, which has similar substrate specificities[29].

One potential mechanism for these effects is that 14-3-3ε binding protects P-NUDEL from phosphatase attack. Consistent with this hypothesis, yeast two-hybrid screening with NUDEL identified the regulatory subunit A of PP2A phosphatase, PR65α, as a NUDEL-interacting protein. We found that PP2A efficiently dephosphorylated CDK5/p35-phosphorylated P-NUDEL *in vitro* (**Fig. 6b**), an activity that was abrogated in the presence of a universal phosphatase inhibitor (NaF) or a PP2A inhibitor (okadaic acid). Notably, 14-3-3ε protected NUDEL from PP2A dephosphorylation in a dose-dependent fashion (**Fig. 6b**). We carried out competition assays to examine the ability of 14-3-3ε to protect P-NUDEL from PP2A dephosphorylation in the presence of various concentrations of non-phosphorylated NUDEL (**Fig. 6c**). One-hundred-fold excess of non-phosphorylated NUDEL was required for PP2A dephosphorylation of 50% of P-NUDEL in the presence of 14-3-3ε. LIS1 binds to a region of NUDEL distinct from the phosphorylation sites (see **Fig. 5a**) and did not afford protection to P-NUDEL from PP2A *in vitro* (data not shown). Taken together, these results indicate that 14-3-3ε selectively binds P-NUDEL and is important in its metabolism and the maintenance of its CDK5/p35 phosphorylation status.

14-3-3ε is required for normal NUDEL, LIS1 and β-COP localization

If NUDEL binding by 14-3-3ε is functionally important, then loss of 14-3-3ε should result in dynein motor function defects similar to those seen in mutants with reduced levels of LIS1 or after inhibition of NUDEL or CDK5/p35 (refs. 14,15,30,31). For example, reduction of LIS1 dosage altered distribution of LIS1 and NUDEL as well as localization of β-COP, a Golgi marker whose distribution is affected by cytoplasmic dynein function[14,15,30].

We examined the localization of NUDEL, LIS1 and β-COP in embryonic (E15.5) cortical neuron cultures from brains of wild-type (*Ywhae*$^{+/+}$) or 14-3-3ε-deficient (*Ywhae*$^{-/-}$) mice. NUDEL and LIS1 were initially present in the centrosome or microtubule organizing center immediately after plating (data not shown) and after 2 d in culture, they were distributed in the soma and throughout the neurites of *Ywhae*$^{+/+}$ neurons (**Fig. 7a**,**c**,**g**,**i**), as expected[14]. In *Ywhae*$^{-/-}$ neurons, however, NUDEL (**Fig. 7d**,**g**) and LIS1 (**Fig. 7f**,**i**) were distributed more prominently in the soma. The distribution of β-COP was diffusely disorganized in the neurites of *Ywhae*$^{-/-}$ neuronal cells (**Fig. 7e**,**h**) compared with its tight perinuclear localization in *Ywhae*$^{+/+}$ cells (**Fig. 7b**,**h**). Defective localization of NUDEL (**Fig. 7j–l**,**p**) and β-COP (**Fig. 7m–o**,**q**) was rescued by transfection of *Ywhae*$^{-/-}$ neurons with 14-3-3ε tagged with green fluorescent protein (GFP). Similar results were found in MEFs (data not shown).

We next determined whether the localization pattern of NUDEL-GFP or NUDEL-GFP with triple amino-acid substitutions at S198A, T219A and S231A (mutant NUDEL-GFP) was affected in E15.5 cortical neurons by inhibition of CDK5 and phosphatase by roscovitine and okadaic acid, respectively. As neurons were transfected after 3 d in culture, NUDEL-GFP was distributed throughout the soma and the neurites in more than 60% of *Ywhae*$^{+/+}$ neurons 2 d after transfection (**Fig. 7r**,**d′**). In *Ywhae*$^{-/-}$ neurons, NUDEL-GFP was concentrated in the soma in 40% of the cells but peripherally distributed to the neurites in only 15% of cells (**Fig. 7s**,**d′**). Treatment with roscovitine inhibited the peripheral distribution of NUDEL-GFP in *Ywhae*$^{+/+}$ neurons (**Fig. 7t**,**d′**) without affecting the distribution in neurons from *Ywhae*$^{-/-}$ mice (**Fig. 7u**,**d′**). Treatment with okadaic acid, however, resulted in apparent rescue of NUDEL-GFP distribution in *Ywhae*$^{-/-}$ neurons (**Fig. 7w**,**d′**) without effects in *Ywhae*$^{+/+}$ neurons (**Fig. 7v**,**d′**). These changes were obvious when examining the percentage of cells with different patterns of NUDEL-GFP distribution (**Fig. 7d′**). By contrast, mutant NUDEL-GFP was similarly localized throughout the soma and neurites irrespective of genotype and treatment (**Fig. 7x–c′**,**e′**), indicating that the effects of the inhibitors were not the result of non-specific effects. These *in vivo* results are consistent with an important role for 14-3-3ε in regulating dynein motor function through binding to P-NUDEL and protection from dephosphorylation.

© 2003 Nature Publishing Group http://www.nature.com/naturegenetics

DISCUSSION

Here, we show that 14-3-3ε is essential for normal brain development and neuronal migration in a dose-dependent fashion. These functions can be linked to two complexes required for neuronal migration: LIS1/NUDEL/dynein and CDK5/p35. Mice heterozygous with respect to both *Pafah1b1* and *Ywhae* had more severe brain defects than mice heterozygous with respect to either gene individually, and human deletion data were consistent with the pivotal role of 14-3-3ε in MDS.

The 14-3-3 protein family is highly conserved and ubiquitously expressed with high levels in the brain, and its members function as regulatory proteins that interact with a wide range of target phosphoproteins, so they may have redundant functions. But certain isoforms of 14-3-3 proteins seem to bind preferentially to particular targets[24,32,33], and genes encoding various 14-3-3 proteins are expressed in differential patterns during development, although all seem to be expressed in the brain (for review, see refs. 20,22). In *D. melanogaster*, 14-3-3 proteins are important for neuronal differentiation. The gene encoding 14-3-3ε is non-essential and is required for RAS/MAPK signaling in the eye[34]. Homozygous-null mutants with respect to the gene *leonardo* (encoding 14-3-3ζ) in *D. melanogaster* die as mature embryos with defects in synaptic vesicle dynamics[35], and low levels of expression of *leonardo* in mushroom bodies result in olfactory learning deficits[36]. This raises the possibility that there are at least some isoform-specific and non-redundant functions in the central nervous system of eukaryotes. Our data are consistent with this possibility, as the absence of 14-3-3ε results in the disruption of neuronal development, migration and survival. A unique role for 14-3-3ε is also supported by NUDEL co-immunoprecipitation experiments with the pan-14-3-3 antibody (**Fig. 5f**) indicating that 14-3-3ε preferentially binds NUDEL.

Neuronal migration is a complicated process that is regulated at several levels by at least three independent but partially overlapping pathways or complexes: the reelin pathway, the CDK5/p35 complex and the LIS1 complex. The CDK5/p35 and CDK5/p39 kinase complexes have an integrating function during neuronal migration, whereas the LIS1 complex regulates dynein motor function. LIS1 is part of a conserved pathway that regulates nuclear movement through dynein activity[30,31,37,38] by binding CDHC and NUDEL[14,15] as well as the light-intermediate chain through mNudE[39]. The activity of this complex is regulated by phosphorylation of NUDEL through CDK5 (refs. 14,15). Presumably, modification of NUDEL by CDK5/p35 phosphorylation changes its affinity for other proteins, such as the CDHC subunit, to regulate activity or motility, as the region of NUDEL containing the phosphorylation sites is required for CDHC binding[14].

14-3-3ε provides an additional molecular and functional link between the LIS1 pathway and CDK5/p35 in neuronal development and migration. NUDEL, 14-3-3ε, CDK5/p35 and LIS1 all seem to have positive effects on dynein motor function and the LIS1 pathway of neuronal migration. This conclusion is derived from loss-of-function studies[8,16,17], inhibitor and overexpression studies[14,15,31] and studies presented here. Our data provide additional evidence for the importance of NUDEL phosphorylation and 14-3-3ε in the LIS1 pathway and dynein motor function.

We provide some evidence that 14-3-3ε may act by protecting P-NUDEL from PP2A. A PP2A regulatory subunit binds to NUDEL. *In vitro* studies identified the protective effect of 14-3-3ε on P-NUDEL against PP2A attack. We tested the possibility that PP2A phosphatase could be relevant *in vivo* by using the phosphatase inhibitor okadaic acid. Treatment of neurons lacking 14-3-3ε with okadaic acid rescued the mislocalization of NUDEL-GFP, an effect that required the three CDK5 S/T sites on NUDEL. Thus, PP2A is a good candidate for an important NUDEL phosphatase in the cell. PP2A dephosphorylates CDK5/p35 sites in several proteins[40,41], it is present on microtubules[42,43] and its deficiency results in dissociation of the nuclear and centrosome cycles in *D. melanogaster*[44]. Although a role for PP2A in neuronal migration has not previously been shown, mice deficient for the catalytic subunit of PP2A die during early embryogenesis[45].

NUDEL is an important target of 14-3-3ε binding, but many other proteins are potential binding partners for 14-3-3ε. For example, it is known that CDK5/p35 regulates cell-cell adhesion molecules and phosphorylates a number of microtubule associated proteins (reviewed in ref. 12). mNudE contains the same Ser/Thr residues as NUDEL[39] and may also be a CDK5 substrate. Any protein phosphorylated by the CDK5/p35 complex is a potential binding partner for 14-3-3ε and could be important for the regulation of neuronal migration and survival by 14-3-3ε.

MDS consists of the most severe grades of lissencephaly, characteristic facial anomalies and occasionally other malformations. The disorder is usually fatal in early childhood, except for rare mild forms. ILS is more heterogeneous with variable lissencephaly (grades 2–4, mainly 3 and 4) and no other malformations. Our data implicate *YWHAE* in the greater severity of neuronal migration defects observed in individuals with MDS and suggest that the complete agyria seen in this syndrome may be the consequence of the heterozygous deletion of *PAFAH1B1* and *YWHAE*, two genes required for optimal neuronal migration. Deletion up to but not including *YWHAE* is compatible with normal brain function. Additionally, deletions including *YWHAE* (and other genes such as *MYO1C* and *CRK*) but not *PAFAH1B1* result in mental retardation without lissencephaly[25]. This latter finding suggests that the locus *YWHAE* may be important in mental retardation, and this is consistent with the defects observed in *Ywhae* mutant mice (K.T. and A.W.-B., unpublished data). The human data collected to date are correlative and cannot formally prove a role for *YWHAE* in these phenotypes. In addition, the deletion data cannot rule out that *CRK*, the gene adjacent to *YWHAE*, is also involved in the MDS phenotype (see **Fig. 1**; ref. 25). *CRK* encodes an adaptor signaling protein that has a role in cell proliferation, differentiation and migration[46,47], as well as axonal growth[48]. No mouse knock-out has been described. Although *CRK* may also participate in neuronal migration, our studies in the mouse assign a definitive role for 14-3-3ε in neuronal migration and imply an important role in the brain phenotype of MDS.

We can propose a molecular model to explain the greater severity of neuronal migration defects observed in MDS. In the wild type, LIS1 binds to NUDEL regardless of its phosphorylation status. 14-3-3ε binds to P-NUDEL at the CDK5 phosphorylation site and protects this site from phosphatase attack, perhaps from PP2A. This stabilizes P-NUDEL, which then binds to CDHC near the site of phosphorylation to promote dynein motor function. In the absence of 14-3-3ε, there is less protection of P-NUDEL from phosphatase attack, and less P-NUDEL to bind normal amounts of LIS1 and CDHC, resulting in lower dynein motor activity. When LIS1 dosage is reduced in individuals with ILS, there is less LIS1 to bind to normal amounts of P-NUDEL to form a complex with the CDHC and promote dynein function. When both proteins are reduced in individuals with MDS, the combined effect of reduction of LIS1 and P-NUDEL from reduction in 14-3-3ε results in even fewer functional CDHC complexes, and mice with these deficiencies have the most severe phenotype.

The proximity of two genes, *PAFAH1B1* and *YWHAE*, in the same genomic region of human and mouse that have dosage-dependent loss-of-function phenotypes in the same developmental pathway regulating neuronal development suggests that this genomic linkage may have functional importance. It is unclear if genes other than *PAFAH1B1* through *YWHAE* in the MDS region contribute to the neuronal or extraneuronal phenotypes of individuals with MDS. For example, the identification of other genes in this region that can contribute to the craniofacial defects seen in MDS will require further study. Based on our studies, the combined use of mouse models and human deletion studies will probably help to identify these genes.

METHODS

Generation of 14-3-3ε-deficient mice. We generated ES cells deficient in *Ywhae* (encoding 14-3-3ε) using a previously described construct[49], except we used PGK-*neo* instead of a *hyg*-positive selectable marker. We injected targeted ES cells into C57BL/6J blastocysts and obtained germline transmission. We maintained heterozygous mutant mice in both mixed 129/S6 × NIH Black Swiss and inbred 129/S6 backgrounds. For Southern-blot analysis, we digested tail DNA with *Bgl*II, separated it on a 0.8% agarose gel and transferred it to Hybond N+ (Amersham). We probed the transferred membrane with a 500-bp *Hin*dIII/*Bam*HI fragment to detect a 4.4-kb wild-type allele or a 3.0-kb mutated allele. We used PCR for routine genotyping of tail DNA (from E14.5 to adulthood) or yolk sac DNA (E12.5 or E13.5 embryos). The primer sequences and conditions for genotyping are available on request. All animal experiments were carried out under protocols approved by the US National Human Genome Research Institute and the National Institutes of Health and the University of California San Diego Animal Care and Use Committees and following guidelines of the US National Institutes of Health.

Histology and immunohistochemistry. We fixed brains of adult mice by perfusion with 4% paraformaldehyde in phosphate-buffered saline (PBS), dissected them and placed them in 4% paraformaldehyde in PBS overnight. We saturated fixed brains with 20% sucrose in PBS overnight at 4 °C and cut them into 40-μm sections with a frozen sliding microtome. We dissected embryos and fixed them with 4% paraformaldehyde in PBS overnight at 4 °C. We embedded fixed embryos in paraffin and sectioned them at 6 μm on a microtome. We embedded brains from E18.5 embryos in optimal cutting temperature (OCT; Tissue-Tek) compound and sectioned them at 14 μm on a cryostat. For immunohistochemistry, we incubated sections in PBS with 5% normal goat serum and 0.01% Triton-X 100 for 20 min at room temperature. We used antibody to Tst-1 (ref. 26; provided by M.G. Rosenfeld, UCSD School of Medicine) at 1:1,000 in PBS with 3% normal goat serum and 0.5% Tween 20. After overnight incubation at 4 °C, we incubated sections with 5 μg ml^{-1} of biotinylated goat secondary antibody to rabbit IgG (Vector) in 1.5% normal goat serum in PBS for 1 h at room temperature and then used the peroxidase-conjugated ABC kit (Vector). We visualized signals with diaminobenzidine. We measured average cortical thickness on 10 sections each of the brains of 4–6 mice stained by Nissl or hematoxylin and eosin.

BrdU birthdating. Pregnant dams from timed matings were injected intraperitoneally at E13.5, E14.5 and E15.5 with 100 mg g^{-1} BrdU (Sigma) and then dissected at E18.5. We processed embryos for paraffin embedding, cut them at 4–5 μm and pretreated them with 10 mM citrate buffer (pH 6.0) for 10 min, boiling in microwave for antigen retrieval. We blocked pretreated sections with 3% normal goat serum in 0.5 % Triton-X 100 in PBS for 30 min at room temperature and stained them with monoclonal antibody to BrdU (1:50; Becton Dickinson) in 3% normal goat serum in 0.5% Tween 20 in PBS and then with biotinylated goat secondary antibody to mouse IgG (1:100; Sigma) in PBS with 1.5% normal goat serum. We visualized BrdU-labeled cells with peroxidase-conjugated ABC kit (Vector) and diaminobenzidine with metal enhancer (Sigma) and counterstained them with hematoxylin. We quantified migration by dividing a 200-μm-wide area of matched E18.5 cortex sections into 10-μm-deep bins and counting the number of labeled cells per bin. Only strongly BrdU-positive cells were counted for analysis, as these represent cells that became post-mitotic soon after BrdU injection. Lightly labeled cells, generated by dilution of BrdU by the following progenitor cell divisions, were not counted. We converted raw numbers in each bin into percentages of total numbers of labeled cells, and the results are represented by a histogram. We analyzed 10 sections each of 4 mice per genotype. We determined the average migration distance of neurons in the same sections and areas of migration assay, and values are presented as mean ± s.e.m. Data were analyzed by ANOVA with the Bonferroni correction.

Yeast two-hybrid analysis. We conjugated full-length NUDEL cDNA to pLexA (Clontech) and used it to screen a fetal mouse brain cDNA library as described[14]. To identify the site of binding of NUDEL with 14-3-3ε, we cloned several truncated cDNAs of NUDEL into pLexA. To produce full-length or truncated NUDEL, we cloned *Bcl*I–*Not*I (amino acids 1–345), *Sma*I–*Not*I (104–345), *Bgl*II–*Not*I (256–345), *Eco*RV–*Not*I (291–345), *Bcl*I–*Pst*I (1–63), *Rsa*I–*Rsa*I (56–166), *Bcl*I–*Tsp*45I (1–189) or *Bcl*I–*Bgl*II (1–256) fragments into pLexA vector. We generated mutant NUDEL proteins conjugated to pLexA using Quick-Change (Stratagene). We generated the LIS1-pLexA plasmid and measured *lacZ* activity as described[14].

Production of recombinant proteins and phosphorylation by CDK5/p35. We expressed GST-tagged recombinant NUDEL protein in bacteria using pGEX4T (Pharmacia) and then purified it on glutathione-sepharose 4B (Pharmacia). We expressed His-tagged recombinant 14-3-3ε, LIS1, CDK5 and p35 in High Five (Invitrogen) using Fast Bac baculovirus expression system (Invitrogen) and then purified it using metal affinity resin (Talon; Clontech). We incubated 10 μg of recombinant NUDEL with 0.5 μg of recombinant CDK5/p35 in 50 μl of 50 mM morpholinopropanesulfonic acid (pH 7.2), 6 mM $MgCl_2$, 1 mM ATP and 4 μCi [γ-^{32}P] ATP for 1 h at 30 °C. NUDEL was collected after incubation by adding an equal volume of 90% ammonium sulfate and then centrifuged at 15,000 r.p.m. for 10 min. The pellet was resuspended in 25 mM Tris-HCl at 1 mg ml^{-1}.

***In vitro* binding assay.** We incubated 1 μg of each GST-tagged recombinant NUDEL protein with 1 μg of His-tagged recombinant 14-3-3ε in 25 mM Tris-HCl (pH 8.0), 140 mM NaCl, 0.1% Triton X-100 overnight. We retrieved His-tagged 14-3-3ε bound to GST-tagged NUDEL (**Fig. 5d**) or GST-tagged NUDEL bound to His-tagged 14-3-3ε (**Fig. 5e**) by binding to glutathione-sepharose beads or Ni beads, respectively, at 4 °C for 1 h. After extensive washing of GST-fusions and bound proteins in the same buffer used for incubation, we separated proteins by SDS–PAGE and visualized them by Coomassie brilliant blue staining or immunoblotting with antibody to His or to GST. The Coomassie-stained filter was subjected to autoradiography.

Immunoprecipitation. We seeded E14.5 MEFs (1×10^6) from wild-type or 14-3-3ε-deficient mutant mice on 10-cm plates. For immunoprecipitation, we lysed labeled cells in 500 μl of 10 mM HEPES buffer (pH 7.4), 2 mM $MgCl_2$, 0.1% Triton X-100, 150 mM NaCl, Protease Inhibitor Cocktail (Roche), 10 mM glycerophosphate-Na and 1 mM sodium vanadate. We added 5 μg of C-6 NUDEL antibody[14] to 500 μg of lysate and incubated it overnight at 4 °C. We retrieved antibody-bound NUDEL by binding to protein A–sepharose beads at 4 °C for 8 h. After extensive washing in lysis buffer, bound NUDEL was released, separated by SDS–PAGE, and immunoblotted using antibody to NUDEL.

Dephosphorylation assays with PP2A. We used phosphorylated NUDEL for a substrate of PP2A (CALBIOCHEM). We incubated 1 μg of substrate in 0.5 U PP2A, 40 mM Tris-HCl (pH 7.4), 20 mM $MgCl_2$, 10 mM $MnCl_2$, 0.04% bovine serum albumin, 0.1 mM dithiothreitol, 0.1 mM EGTA and Protease Inhibitor Cocktail (Roche) at 30 °C for 30 min. After incubation, we separated the reaction mixture by SDS–PAGE and then carried out immunoblotting with antibody to NUDEL and autoradiography. Radioactivity was measured by Phospho-Imager (BAS2000; Fuji).

NUDEL–GFP expression vectors. We cloned a blunt-ended *Bcl*I–*Hpa*I fragment of NUDEL into the blunt-ended *Age*I site of pEGFP C1 (Clonetech). We introduced Ser/Thr-to-Ala mutations by the Quick-Change site-directed mutagenesis kit (Stratagene).

© 2003 Nature Publishing Group http://www.nature.com/naturegenetics

Immunoprecipitation and western-blot analysis. We homogenized brains or MEFs in lysis buffer (10 mM Tris-HCl pH 7.3, 100 mM NaCl, 20 mM KCl and 0.1 % Nonidet P-40 supplemented with protease inhibitor cocktail (Roche), 1 mM NaF and 1 mM sodium vanadate). We incubated 500 μg of lysate with 10 μg of C-6 antibody to NUDEL and precipitated it with protein G–separose. After extensive washing, we eluted interacting proteins and separated them by SDS–PAGE. We detected LIS1 (sc-7577 antibody; Santa Cruz) and 14-3-3 isoforms (pan-14-3-3 antibody; Santa Cruz). We generated the P-NUDEL antibody against the phosphorylated Ser231. We injected a KLH-coupled peptide (TENTFPpSPKAIPC) into a rabbit. The serum was first subjected to affinity purification against a non-phosphorylated peptide and then the flow-through was further purified in a phospho-peptide column. Finally, the purified antibody was shown to recognize P-NUDEL phosphorylated at Ser231.

Primary cell culture, transfection and immunofluorescence. For E15.5 cortical neuronal cells, we treated minced cortices with 2.2 mg ml^{-1} papain (Worthington Biochemical) in Earle's balanced salt solution (GIBCO BRL) with 0.5 mM EDTA and 0.13 mg ml^{-1} cysteine for 15 min at 37 °C. After centrifugation, supernatants were treated with 0.001% DNase (Worthington Biochemical) in Earle's balanced salt solution supplemented with 10 mg ml^{-1} bovine serum albumin (Roche) and 10 mg ml^{-1} trypsin inhibitor (Sigma) for 5 min at room temperature. After centrifugation, we plated cortical neuronal cells with Neurobasal medium (GIBCO BRL) supplemented with 2% B27 (GIBCO BRL) and 50 μg ml^{-1} gentamycin at 37 °C in 5% carbon dioxide/95% air for 2–3 d. We detected neuronal cells using antibody to class III β-tubulin (BabCO), and >95% of cells were neuronal cells (data not shown). No obvious genotype or treatment differences were observed using this antibody.

For immuncytochemistry, we cultured 1×10^5 cells on coverslips coated with 50 μg ml^{-1} poly-L-lysine (Sigma) overnight at room temperature and then incubated them with 10 μg ml^{-1} laminin (Sigma) for 1 h at room temperature in 24-well plate. After 2 d in culture, we washed cells with PBS and fixed them with ice-cold methanol or acetone for 2 min. After blocking with 4% donkey normal serum (Jackson Immunoresearch) for 20 min at room temperature, we incubated cells with various primary antibodies overnight at 4 °C or for 1 h at room temperature. We used goat antibody to LIS1 (Santa Cruz) and mouse antibody to β-COP (Sigma) at 1:100 and 1:80 in 1.5% donkey normal serum in PBS, respectively. We used antibody to NUDEL C-6 at 1:50. After washing 4 times with PBS, we used Rhodamine Red–labeled donkey antibody to rabbit IgG, tetramethyl rhodamine isothiocyanate–labeled donkey antibody to goat IgG or fluorescein isothiocyanate–labeled donkey antibody to mouse IgG secondary antibodies (Jackson Immunoresearch) at 1:200 in 1.5% donkey normal serum in PBS for 30 min at room temperature. We visualized nuclei with 300 nM DAPI and mounted them with Prolonged antifade kit.

For transfection, we cultured 1.5×10^5 cortical neuronal cells on coverslips treated with both poly-L-lysine and laminin in 24-well plates. After 3 d in culture, we transfected cells with 2 μg 14-3-3ε–GFP fusion protein in 2 μl LIPOFECTAMINE 2000 reagents in 100 μl OPTI-MEM media without fetal bovine serum for 24 h, resulting in 20% transfection efficiency.

For quantification of distribution pattern of NUDEL, LIS1, β-COP, NUDEL-GFP and mutant NUDEL-GFP, we analyzed 100 cells of preparations from each of 2–3 mice per genotype and classified them into two (for β-COP) or four (for other antibodies) categories as indicated in figure legends. The criteria for scoring the cells for localization in soma, neurites and centrosome are as follows: soma, signals appear only around nuclei, sometimes as dots because neurons have small cytoplasm (see **Fig. 7d**); neurites, signals were only in neurites, not around nuclei at all; soma and neurites, signal was seen in both places; centrosome, signals appeared as one or two small dots, not more than three dots; punctate, cells with more than three dots after transfection. For β-COP: diffuse, signals were apparent around nuclei and in neurites in the same cell (as in **Fig. 7e**); peri-nuclear, signals were only tightly surrounding the nucleus (as in **Fig. 7b**). In fixed cells, or in transfected cells expressing GFP, we took photos with the same shutter speed with the charge-coupled device camera for each individual experiment. These photo sets still included various intensities of signals even if they came from same staining and culture conditions. We selected for analysis cells that had the same or similar intensities and a healthy cellular morphology (single smooth nuclei, well attached to the plate and non-senescent in appearance). We excluded cells with saturated signals.

We treated cells with 1 μM roscovitine[15] or 10 nM okadaic acid for 2 d to inhibit CDK5 or PP2A, respectively. The concentration of okadaic acid was chosen to selectively inhibit PP2A based on sensitivity to apoptosis, IC80 data and cell data (for review, see ref. 50).

ACKNOWLEDGMENTS
We would like to thank P. LaPorte and J. Chung for technical support; J. Gleeson, M.G. Rosenfeld and M. Muramatsu for reagents and for providing valuable suggestions and discussion; and S. Hisanaga for providing baculoviruses of CDK5 and p35. A.W-B., D.H.L. and W.B.D. were supported by grants from the US National Institutes of Neurological Diseases and Stroke, an institutional grant from the Howard Hughes Medical Institute and University of California San Diego School of Medicine funds. S.H. was supported by PRESTO, Japan Science and Technology Corporation. M.J.G. was a physician research fellow of the Howard Hughes Medical Institute.

COMPETING INTERESTS STATEMENT
The authors declare that they have no competing financial interests.

Received 31 January; accepted 6 May 2003
Published online 8 June 2003; doi:10.1038/ng1169

1. Dobyns, W.B., Reiner, O., Carrozzo, R. & Ledbetter, D.H. Lissencephaly. A human brain malformation associated with deletion of the *LIS1* gene located at chromosome 17p13. *J. Am. Med. Assoc.* **270**, 2838–2842 (1993).
2. Dobyns, W.B., Curry, C.J., Hoyme, H.E., Turlington, L. & Ledbetter, D.H. Clinical and molecular diagnosis of Miller–Dieker syndrome. *Am. J. Hum. Genet.* **48**, 584–594 (1991).
3. Dobyns, W.B., Elias, E.R., Newlin, A.C., Pagon, R.A. & Ledbetter, D.H. Causal heterogeneity in isolated lissencephaly. *Neurology* **42**, 1375–1388 (1992).
4. Ledbetter, S.A., Kuwano, A., Dobyns, W.B. & Ledbetter, D.H. Microdeletions of chromosome 17p13 as a cause of isolated lissencephaly. *Am. J. Hum. Genet.* **50**, 182–189 (1992).
5. Chong, S.S. *et al.* A revision of the lissencephaly and Miller–Dieker syndrome critical regions in chromosome 17p13.3. *Hum. Mol. Genet.* **6**, 147–155 (1997).
6. Reiner, O. *et al.* Isolation of a Miller–Dieker lissencephaly gene containing G protein β-subunit-like repeats. *Nature* **364**, 717–721 (1993).
7. Lo Nigro, C. *et al.* Point mutations and an intragenic deletion in *LIS1*, the lissencephaly causative gene in isolated lissencephaly sequence and Miller–Dieker syndrome. *Hum. Mol. Genet.* **6**, 157–164 (1997).
8. Hirotsune, S. *et al.* Graded reduction of Pafah1b1 (Lis1) activity results in neuronal migration defects and early embryonic lethality. *Nat. Genet.* **19**, 333–339 (1998).
9. Gambello, M.J. *et al.* Multiple dose dependent effects of *Lis1* on cerebral cortical development. *J. Neurosci.* **23**, 1719–1729 (2003).
10. Cahana, A. *et al.* Targeted mutagenesis of *Lis1* disrupts cortical development and LIS1 homodimerization. *Proc. Natl. Acad. Sci. USA* **98**, 6429–6434 (2001).
11. Wynshaw-Boris, A. & Gambello, M.J. LIS1 and dynein motor function in neuronal migration and development. *Genes Dev.* **15**, 639–651 (2001).
12. Gupta, A., Tsai, L.-H. & Wynshaw-Boris, A. Life is a journey: a genetic look at neocortical development. *Nat. Rev. Genet.* **3**, 342–355 (2002).
13. Morris, R.N. Nuclear migration: from fungi to the mammalian brain. *J. Cell Biol.* **148**, 1097–1101 (2000).
14. Sasaki, S. *et al.* A LIS1/NUDEL/cytoplasmic dynein heavy chain complex in the developing and adult nervous system. *Neuron* **28**, 681–696 (2000).
15. Niethammer, M. *et al.* NUDEL is a novel Cdk5 substrate that associates with LIS1 and cytoplasmic dynein. *Neuron* **28**, 697–711 (2000).
16. Oshima, T. *et al.* Targeted disruption of the cyclin-dependent kinase 5 gene results in abnormal corticogenesis, neuronal pathology and perinatal death. *Proc. Natl. Acad. Sci. USA* **93**, 11173–11178 (1996).
17. Chae, T. *et al.* Mice lacking p35, a neuronal specific activator of Cdk5, display cortical lamination defects, seizures, and adult lethality. *Neuron* **18**, 29–42 (1997).
18. Pilz, D.T. *et al.* *LIS1* and *XLIS* (*DCX*) mutations cause most classical lissencephaly, but different patterns of malformation. *Hum. Mol. Genet.* **7**, 2029–2037 (1998).
19. Cardoso, C. *et al.* The location and type of mutation predict malformation severity in isolated lissencephaly caused by abnormalities within the *LIS1* gene. *Hum. Mol. Genet.* **9**, 3019–3028 (2000).
20. Fu, H., Subramanian, R.R. & Masters, S.C. 14-3-3 proteins: structure, function, and regulation. *Annu. Rev. Pharmacol. Toxicol.* **40**, 617–647 (2000).
21. Muslin, A.J. & Xing, H. 14-3-3 proteins: regulation of subcellular localization by molecular interference. *Cell. Signal.* **12**, 703–709 (2000).
22. Tzivion, G. & Avruch, J. 14-3-3 proteins: active cofactors in cellular regulation by serine/threonine phosphorylation. *J. Biol. Chem.* **277**, 3061–3064 (2002).
23. Muslin, A.J., Tanner, J.W., Allen, P.M. & Shaw, A.S. Interaction of 14-3-3 with signaling proteins is mediated by the recognition of phosphoserine. *Cell* **84**, 889–897 (1996).
24. Yaffe, M.B. *et al.* The structural basis for 14-3-3:phosphopeptide binding specificity. *Cell* **91**, 961–971 (1997).
25. Cardoso, C. *et al.* Refinement of a 400 kb critical region allows genotypic differentiation between isolated lissencephaly, Miller–Dieker syndrome and other phenotypes secondary to deletions of 17p13.3. *Am. J. Hum. Genet.* **72**, 918–930 (2003).

© 2003 Nature Publishing Group http://www.nature.com/naturegenetics

26. Bermingham, J. *et al.* Tst-1/Oct-6/SCIP regulates a unique step in peripheral myelination and is required for normal respiration. *Genes Dev.* **10**, 1751–1762 (1996).
27. Fleck, M.W. *et al.* Hippocampal abnormalities and enhanced excitability in a murine model of human lissencephaly. *J. Neurosci.* **20**, 2439–2450 (2000).
28. Huang, D., Patrick, G., Moffat, J., Tsai, L.H. & Andrews, B. Mammalian Cdk5 is a functional homologue of the budding yeast Pho85 cyclin-dependent protein kinase. *Proc. Natl. Acad. Sci. USA* **96**, 14445–14450 (1999).
29. Floyd, S.R. *et al.* Amphiphysin 1 binds the cyclin-dependent kinase (cdk) regulatory subunit p35 and is phosphorylated by dck5 and cdk2. *J. Biol. Chem.* **276**, 8104–8110 (2001).
30. Smith, D.S. *et al.* Regulation of cytoplasmic dynein behaviour and microtubule organization by mammalian Lis1. *Nat. Cell Biol.* **2**, 767–775 (2000).
31. Yan, X. *et al.* Human Nudel and NudE as regulators of cytoplasmic dynein in poleward protein transport along the mitotic spindle. *Mol. Cell Biol.* **23**, 1239–1250 (2003).
32. Vincenz, C. & Dixit, V.M. 14-3-3 proteins associate with A20 in an isoform-specific manner and function both as chaperone and adapter molecules. *J. Biol. Chem.* **271**, 20029–20034 (1996).
33. Van Der Hoeven, P.C., Van Der Wal, J.C., Ruurs, P., Van Dijk, M.C. & Van Blitterswijk, J. 14-3-3 isotypes facilitate coupling of protein kinase C-zeta to Raf-1: negative regulation by 14-3-3 phosphorylation. *Biochem. J.* **345**, 297–306 (2000).
34. Chang, H.C. & Rubin, G.M. 14-3-3 epsilon positively regulates Ras-mediated signaling in *Drosophila. Genes Dev.* **11**, 1132–1139 (1997).
35. Broadie, K., Rushton, E., Skoulakis, E.M. & Davis, R.L. Leonardo, a *Drosophila* 14-3-3 protein involved in learning, regulates presynaptic function. *Neuron* **19**, 391–402 (1997).
36. Skoulakis, E.M. & Davis, R.L. Olfactory learning deficits in mutants for *leonardo*, a *Drosophila* gene encoding a 14-3-3 protein. *Neuron* **17**, 931–944 (1996).
37. Faulkner, N.E. *et al.* A role for the lissencephaly gene *LIS1* in mitosis and cytoplasmic dynein function. *Nat. Cell Biol.* **2**, 784–791 (2000).
38. Liu, Z., Steward, R. & Luo, L. *Drosophila* Lis1 is required for neuroblast proliferation, dendritic elaboration and axonal transport. *Nat. Cell Biol.* **2**, 776–783 (2000).
39. Feng, Y. *et al.* Interactions between LIS1 and mNudE, a central component of the centrosome, are required for CNS lamination. *Neuron* **28**, 665–679 (2000).
40. Veeranna *et al.* Neuronal cyclin-dependent kinase-5 phosphorylation sites in neurofilament protein (NF-H) are dephosphorylated by protein phosphatase 2A. *J. Neurochem.* **64**, 2681–2690 (1995).
41. Sontag, E. *et al.* Regulation of the phosphorylation state and microtubule-binding activity of Tau by protein phosphatase 2A. *Neuron* **17**, 1201–1207 (1996).
42. Price, N.E., Wadzinski, B. & Mumby, M.C. An anchoring factor targets protein phosphatase 2A to brain microtubules. *Brain Res. Mol. Brain Res.* **73**, 68–77 (1999).
43. Sontag, E. *et al.* Molecular interactions among protein phosphatase 2A, tau, and microtubules. Implications for the regulation of tau phosphorylation and the development of tauopathies. *J. Biol. Chem.* **274**, 25490–25498 (1999).
44. Lin, F.C. & Arndt, K.T. The role of *Saccharomyces cerevisiae* type 2A phosphatase in the actin cytoskeleton and entry into mitosis. *EMBO J.* **14**, 2745–2759 (1995).
45. Gotz, J., Probst, A., Ehler, E., Hemmings, B. & Kues, W. Delayed embryonic lethality in mice lacking protein phosphatase 2A catalytic subunit Cα. *Proc. Natl. Acad. Sci. USA* **95**, 12370–12375 (1998).
46. Feller, S. *et al.* Physiological signals and oncogenesis mediated through Crk family adapter proteins. *J. Cell Physiol.* **177**, 535–552 (1998).
47. Tsuda, M., Tanaka, S., Sawa, H., Hanafusa, H. & Nagashima, K. Signaling adaptor protein v-Crk activates rho and regulates cell motility in 3Y1 rat fibroblast cell line. *Cell. Growth Differ.* **13**, 131–139 (2002).
48. Weinstein, D.E., Dobrenis, K. & Birge, R.B. Targeted expression of an oncogenic adaptor protein v-Crk potentiates axonal growth in dorsal root ganglia and motor neurons in vivo. *Brain Res. Dev. Brain Res.* **116**, 29–39 (1999).
49. Hirotsune, S. *et al.* Genomic organization of the murine Miller–Dieker/lissencephaly region: conservation of linkage with the human region. *Genome Res.* **7**, 625–634 (1997).
50. Sontag, E. Protein phosphatase 2A: the Trojan Horse of cellular signaling. *Cell. Signal.* **13**, 7–16 (2001).

© 2003 Nature Publishing Group http://www.nature.com/naturegenetics